

# Modeling and Numerical Simulation of Bioheat Transfer and Biomechanics in Soft Tissue \*

Wensheng Shen<sup>†</sup> and Jun Zhang<sup>‡</sup>

Laboratory for High Performance Scientific Computing and Computer Simulation,  
Department of Computer Science, University of Kentucky,  
Lexington, KY 40506-0046, USA

Fuqian Yang<sup>§</sup>

Department of Chemical and Materials Engineering,  
University of Kentucky,  
Lexington, KY 40506-0046, USA

January 27, 2004

## Abstract

A mathematical model describing the thermomechanical interactions in biological bodies at high temperature is proposed by treating the soft tissue in biological bodies as a thermo-poroelastic media. The heat transfer and elastic deformation in soft tissues are examined based on the Pennes bioheat transfer equation and the modified Duhamel-Neuman equations. The three dimensional governing equations based on the proposed model is discretized using a 19 point finite difference scheme. The resulting large sparse linear system is solved by a preconditioned Krylov subspace method. Numerical simulations show that the proposed model works well in the test situations and the proposed numerical techniques are efficient.

**Key words:** Bioheat transfer, biomechanics, discretization, iterative solver.

## 1 Introduction

Diagnosis, surgery, and prosthesis are common medical treatments visible to us, but the biomechanics associated with them may not be as knowledgeable to us as they should be. It would be much better if we could understand the mechanics in living tissues before a medical treatment is applied, as we can do in engineering area by solving constitutive equations. One of the major difficulties in biomechanics is to determine the mechanical properties of materials and tissues under

---

\*Technical Report No. 391-04, Department of Computer Science, University of Kentucky, Lexington, KY, 2004. This research work was supported in part by NSF under grants CCR-9988165, CCR-0092532, ACR-0202934, ACR-0234270, in part by DOE under grant DE-FG02-02ER45961, in part by Kentucky Science & Engineering Foundation under grant KSEF-02-264-RED-002, and in part by the University of Kentucky Research Committee.

<sup>†</sup>E-mail: wensheng@csr.uky.edu.

<sup>‡</sup>Corresponding author. E-mail: jzhang@cs.uky.edu. URL: <http://www.cs.uky.edu/~jzhang>.

<sup>§</sup>E-mail: fyang0@engr.uky.edu.

investigation [1]. Therefore, numerical modeling plays an important role in biomechanics by either solving existing or assisting in determining unknown constitutive equations.

Heat transfer is a very fundamental and important process in living things, especially in human bodies in order to maintain an almost constant temperature. In fact, interesting results related to bioheat transfer have been obtained in the past several decades, such as Pennes bioheat transfer equation [2] and other microstructure bioheat transfer models [3, 4, 5].

The modeling of heat related phenomena such as bioheat transfer and heat-induced stress is useful for the development of biological and biomedical technologies, such as thermotherapy and design of heating or cooling garments. A recent trend in bioheat transfer is the application of heat therapy on tumors due to the fact that heat helps the body against cancer. Such examples are, to list a few, the development of a model-predictive controller (MPC) of the thermal dose in hyperthermia cancer treatments [22], the use of mammary gland tumor for determining the performance parameters of a microwave radiometer [23], the reduction of large-scale, nonlinear ordinary differential equations due to nonlinear models of electromagnetic phased-array hyperthermia [21], three-dimensional finite-element analyses for radio-frequency hepatic tumor ablation [8], and so on. However, there is little study on the thermal mechanical interaction at high temperature even though it is related to the thermal damage of tissue such as skin wrinkle and tissue shrinkage.

In this work, a thermomechanical model is proposed to investigate the thermomechanical interaction of biological bodies subjected to high temperature. The objective of this research is to obtain some quantitative descriptions of the thermomechanical behavior of soft tissue according to the relationship between heat transfer and heat-induced stress, and eventually to apply this useful information in diagnosis, surgery, prosthesis, and other medical interventions. Since the mechanical behavior may be coupled with electrical and biochemical processes, the analysis related to tissue is much more difficult than traditional structural mechanics. As a rudimentary step of the research, some assumptions are made to simplify the analysis:

- (1) Only mechanical response is considered, electrical and biochemical responses are not included.
- (2) The tissue is isotropic, and the thermal and mechanical responses can be uniformly defined.
- (3) Possible mass transfer such as transport of moisture is ignored.

A three-dimensional numerical model is developed to predict the time dependent temperature distribution in biological tissues and the related deformation. In this work, a 19 point finite difference scheme is employed to discretize the displacement equation, while the heat equation is discretized using a 7 point central difference scheme based on the proposed model. We use an iterative method to solve the resultant linear systems. Simulation results are obtained which demonstrate the thermomechanical interactions of soft tissue.

The rest of the paper describes the development of the model that we propose and the numerical methods that we use to solve the model. The mathematical model is introduced in detail in Section 2 for heat transfer process and mechanical analysis. In Section 3, a finite difference scheme is presented for the three dimensional displacement equation, and a preconditioned GMRES

iterative method is employed to solve the large sparse linear systems. Numerical results are reported and discussed in Section 4. Finally, a brief conclusion is given in Section 5.

## 2 Constitutive Equations

### 2.1 Heat transfer process

The heat transfer in soft tissue during the thermal exposure to high temperature can be described using Pennes bioheat equation, which is based on the classical Fourier law of heat conduction [2]. The Pennes model is used to address the heat transfer in living tissues. The model is based on the assumption of the energy exchange between the blood vessels and the surrounding tissues. Even though there may exist some differences in describing bioheat transfer in regimes, where vascular countercurrent heat exchange can possibly skew heat flux and temperature information, Pennes model may provide suitable temperature distributions in whole body, organ, and tumor analysis under study [7]. According to Pennes model, the total energy exchange by the flowing blood is proportional to the volumetric heat flow and the temperature difference between the blood and the tissue. The three dimensional expression of Pennes bioheat equation in a media with uniform material properties is given by

$$\rho C \frac{\partial T}{\partial t} = k \frac{\partial^2 T}{\partial x^2} + k \frac{\partial^2 T}{\partial y^2} + k \frac{\partial^2 T}{\partial z^2} + w_b C_b (T_a - T) + Q_m + Q_r(x, y, z, t), \quad (1)$$

where  $T$  is temperature  $^{\circ}C$ ,  $\rho$  the tissue density  $\text{kg}/\text{m}^3$ ,  $C$  the tissue specific heat  $\text{J}/(\text{kg}^{\circ}C)$ ,  $k$  the tissue thermal conductivity  $\text{W}/(\text{m}^{\circ}C)$ ,  $w_b$  the blood perfusion rate  $\text{kg}/(\text{m}^3\text{s})$ ,  $C_b$  the blood specific heat,  $T_a$  the arterial temperature,  $Q_m$  the metabolic heat generation rate  $\text{W}/\text{m}^3$ , and  $Q_r$  the regional heat sources  $\text{W}/\text{m}^3$ .

In the case of bioheat transfer such as burn injury, the computational domain may be selected as a rectangular box as indicated in Fig. 1. The boundary conditions with respect to Eq. (1) corresponding to the computational domain shown in Fig. 1, where the space in the  $x$  direction starts from the body core ( $x = 0$ ) and ends at the skin surface ( $x = H$ ), can be described as:

- (1) In the  $x$  direction, given temperature boundary condition is applied at the body core, i.e.,  $T = T_c$  at  $x = 0$ ; convective boundary condition is used at the skin surface,  $-k \frac{\partial T}{\partial x} = h_f(T - T_f)$  at  $x = H$ , which is the normal case that the skin surface is subjected to.
- (2) In the  $y$  direction, symmetric boundary conditions are employed on both the starting and ending edges, i.e.,  $-k \frac{\partial T}{\partial y} = 0$  at  $y = 0$ ;  $-k \frac{\partial T}{\partial y} = 0$  at  $y = L$ .
- (3) In the  $z$  direction, again symmetric boundary conditions are enforced, i.e.,  $-k \frac{\partial T}{\partial z} = 0$  at  $z = 0$ ;  $-k \frac{\partial T}{\partial z} = 0$  at  $z = W$ .

The specification of boundary conditions (2) and (3) can be justified as that the heating source are located around the center in the  $y - z$  plane at certain  $x$  position, for example,  $x = h$ , while the four borders parallel to the  $x$  axis in the computational domain are far away from the

heating sources, hence symmetric boundary conditions can be used. The actual dimensions of the computational domain and locations of the heating sources are given in Section 4.

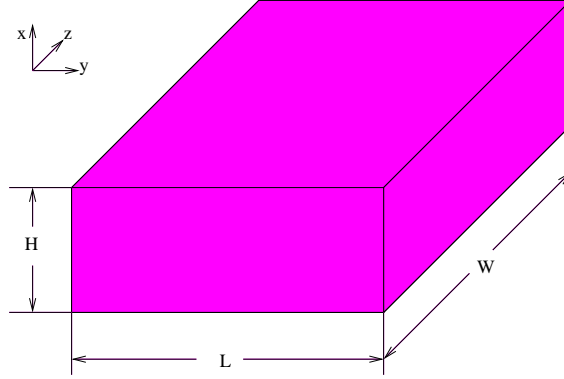


Figure 1: An illustration of the computational domain of a soft tissue.

## 2.2 Stress, strain, and displacement evolution

One of the destructive mechanisms for thermal damage of soft tissue is thermal induced high mechanical stress. To study the thermal induced deformation in soft tissue at high temperature, the thermoporoelasticity model is used in which stress, strain, pressure and temperature are related. The constitutive relation describing the elastic deformation of the soft tissue may be expressed by the modified Duhamel-Numann equation for porous media as [26]

$$\sigma_{ij} = 2G(\varepsilon_{ij} + \frac{\nu}{1-2\nu}\varepsilon_{kk}\delta_{ij}) - \frac{3(\nu_u - \nu)}{B(1+\nu_u)(1-2\nu)}p\delta_{ij} - \frac{2G\alpha(1+\nu)}{1-2\nu}\Delta T\delta_{ij}, \quad (2)$$

where  $\varepsilon_{kk} = \partial u_1/\partial x_1 + \partial u_2/\partial x_2 + \partial u_3/\partial x_3$ ,  $\sigma_{ij}$  and  $\varepsilon_{ij}$  are the second order total stress and average strain tensors ( $i, j = 1, 2, 3$ ) respectively,  $p$  the fluid pressure inside the vasculature, and  $\Delta T$  the temperature difference. The temperature for the tissue and the fluid in capillary beds is considered the same due to the fact that local heat exchange between both the components may be rapid enough in comparison with global heat transfer and fluid flow. Other symbols in Eq. (2) are  $G$  shear modulus,  $\nu$  Poisson's ratio for drained state,  $\nu_u$  Poisson's ratio for undrained state [9],  $B$  Skempton's constant [10],  $\alpha$  thermal expansion coefficient,  $\delta_{ij}$  the Kronecker delta.

If the pressure term is not included, Eq. (2) is reduced to the stress equation in thermoelasticity to calculate thermal stresses [6].

Treat the tissue as the thermoporoelastic media, the equilibrium equation is

$$G(u_{i,jj} + \frac{1}{1-2\nu}u_{j,ji}) - \frac{3(\nu_u - \nu)}{B(1+\nu_u)(1-2\nu)}p_{,i} - \frac{2G\alpha(1+\nu)}{1-2\nu}\Delta T_{,i} = 0, \quad (3)$$

where  $u_i$  is an average displacement vector of the porous matrix and is related to the strain tensor by the equation

$$\varepsilon_{ij} = (u_{i,j} + u_{j,i})/2. \quad (4)$$

The diffusion equation governing the fluid pressure changes in the tissue is

$$\frac{\partial p}{\partial t} = Cp_{,jj}, \quad (5)$$

where

$$C = \frac{2kGB^2(1 + \nu_u)^2(1 - \nu)}{9(1 - \nu_n)(\nu_u - \nu)}. \quad (6)$$

Eqs. (1), (2), (3), and (5) constitute the basic equations to describe the thermomechanical behavior of the soft tissues at high temperature. If the soft tissue is treated as an isotropic elastic medium, the thermal deformation of the soft tissue can be described by thermoelasticity and Eq. (3) becomes [11]

$$G(u_{i,jj} + \frac{1}{1 - 2\nu}u_{j,ji}) - \frac{2G\alpha(1 + \nu)}{1 - 2\nu}\Delta T_{,i} = 0. \quad (7)$$

Thus the model is simplified to a quasi-steady state thermoelasticity problem. Together with boundary conditions, the response of biological bodies to high temperature and the corresponding deformation and stress and strain variations can be determined, from which the location of the thermomechanical damage due to temperature and stresses can be revealed. This will provide us with the necessary information on the approaches to protect biological bodies at high temperature.

### 3 Numerical Techniques

#### 3.1 Finite difference discretization

The thermomechanical interactions due to high temperature can be found by solving Eqs. (1) and (7). It is clear that in the proposed model, Eqs. (1) and (7) are not coupled. The strategy is to solve temperature from Eq. (1) first, then solve displacement from Eq. (7). Eq. (1) is time-dependent, and its solution has already been obtained in our previous work using a Crank-Nicolson scheme based on the standard 7 point central difference discretization [12]. In this article, we will stress on the solution of Eq. (7) using a finite difference scheme. Eq. (7) differs from Eq. (1) by:

- (1) In Eq. (7) the unknown variables are a vector consisting of three components, i.e., displacements in the  $x$ ,  $y$ , and  $z$  space directions, while in Eq. (1) there is only one unknown variable.
- (2) Unlike Eq. (1), there are some mixed derivatives in Eq. (7).
- (3) Eq. (1) is time-dependent, while Eq. (7) is not.

Therefore, it may not be very convenient to discretize Eq. (7) using the standard 7 point central difference scheme, instead, a 19 point finite difference scheme is employed in the discretization of Eq. (7), as

$$\sum_{i=1}^7 a_{i-1}u_{i-1} + \sum_{i=1}^4 a_{i+6}v_{i+6} + \sum_{i=1}^4 a_{9+2i}w_{9+2i} = F_x, \quad (8)$$

$$\sum_{i=1}^7 b_{i-1}v_{i-1} + \sum_{i=1}^4 b_{i+6}u_{i+6} + \sum_{i=1}^4 b_{10+2i}w_{10+2i} = F_y, \quad (9)$$

$$\sum_{i=1}^7 c_{i-1} w_{i-1} + \sum_{i=1}^4 c_{9+2i} u_{9+2i} + \sum_{i=1}^4 c_{10+2i} v_{10+2i} = F_z, \quad (10)$$

where  $a$ ,  $b$ , and  $c$  are coefficients determined by the grid step size as well as the material properties of the medium,  $u$ ,  $v$ , and  $w$  are displacements in the  $x$ ,  $y$ , and  $z$  directions respectively, and  $F_x$ ,  $F_y$ , and  $F_z$  are the body forces in the three spatial directions respectively. The three displacement components in Eq. (7) are expressed explicitly using  $u$ ,  $v$ , and  $w$ , as can be seen in Eqs. (8), (9), and (10). The labeling of the grid points is shown in Fig. 2. Even though it is a 19 point finite difference scheme, only 15 points are used in each of the above 3 equations. For example, points 12, 14, 16, and 18 are not used in Eq. (8), points 11, 13, 15, and 17 not used in Eq. (9), and points 7, 8, 9, and 10 not used in Eq. (10). Without loss of generality, Eqs. (8), (9), and (10) may be

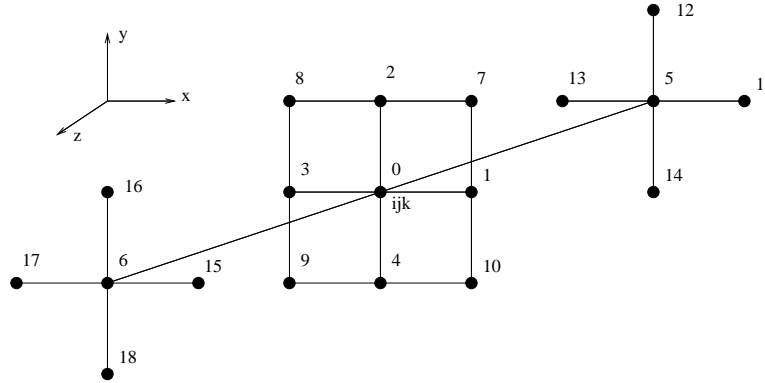


Figure 2: The 19 point finite difference stencil defined in a unit cube.

expressed in the form of  $Ax = b$ , where  $A$  is the coefficient matrix,  $x$  is the unknown vector, and  $b$  is the right hand side. It is worth noticing that the number of rows and number of columns in the resultant matrix  $A$  are triple of the number of internal grid points in a mesh, because of the fact that there are three unknowns at each of the grid point.

### 3.2 Iterative solver

The sparse linear system arising from the discretized equilibrium equation needs to be solved efficiently. Direct solution methods based on Gaussian elimination are prohibitively expensive for such large scale 3D problems in terms of memory cost and CPU time. Thus iterative methods are generally believed to be a more viable means in such situations. In this article, one of the fastest iterative methods, a Krylov subspace method, is employed to solve the resulting linear systems. In order to reduce the number of iterations, a robust preconditioner is used as well. In particular, a linear system solver GMRES, a generalized minimal residual algorithm based on Arnoldi process and implemented with reverse communication, is chosen to do the computation [13].

The convergence rate of GMRES can be improved by a suitable preconditioning technique. For a linear system  $Ax = b$ , the preconditioned system may be written as

$$(M_L^{-1} A M_R^{-1})(M_R x) = M_L^{-1} b, \quad (11)$$

where  $M_L$  and  $M_R$  are left and right preconditioners respectively, and should be inexpensive to compute and easy to invert. The preconditioned linear system (11) itself should be easier to solve iteratively than the original one. If  $M_R = I$ , left preconditioning results. In contrast, if  $M_L = I$ , right preconditioning results. An algorithm describing the procedure of solving  $Ax = b$  using a preconditioned GMRES is presented in the following [14].

**ALGORITHM 3.1 Right Preconditioned GMRES solver.**

1. Assume  $x_0$
2. Compute  $r_0 = b - Ax_0$ ,  $\beta = \|r_0\|_2$ , and  $v_1 = r_0/\beta$
3. For  $j = 1, \dots, m$ , Do:
  5. Compute  $w := AM^{-1}v_j$
  6. For  $i = 1, \dots, j$ , Do:
    7.  $h_{i,j} := (w, v_i)$
    8.  $w := w - h_{i,j}v_i$
  9. End Do
  10. Compute  $h_{j+1,j} = \|w\|_2$  and  $v_{j+1} = w/h_{j+1,j}$
  11. Define  $V_m := [v_1, \dots, v_m]$ ,  $\bar{H}_m = \{h_{i,j}\}_{1 \leq i \leq j+1; 1 \leq j \leq m}$
  12. End Do
13. Compute  $y_m = \operatorname{argmin}_y \|\beta e_1 - \bar{H}_m y\|_2$ , and  $x_m = x_0 + M^{-1}V_m y_m$
14. If convergence criterion is satisfied, then stop, otherwise set  $x_0 = x_m$  and go to 1

As one of the best known preconditioning techniques, incomplete LU factorization is often applied to accelerate the convergence of GMRES, and widely used in solving linear systems resulting from engineering and medical investigations [15, 16]. By neglecting most, or even all, the fill-in terms during the elimination process, the sparsity of the  $L$  and  $U$  factors is preserved in the ILU factorization. The product matrix  $LU$  is then only an approximation of the coefficient matrix. Here, a generic ILU algorithm with thresholding (ILUT) is used to construct the preconditioner for GMRES. More details about Krylov subspace methods and ILU factorization preconditioning techniques can be found in [14].

## 4 Numerical Experiments and Discussion

Two numerical examples, hyperthermia and sinusoidal surface heating, are used to test the validation of the proposed thermomechanical interaction model. The efficiency of ILUT in improving the computational performance is also investigated. In the computation, the geometry size related to Fig. 1 is selected as:  $H = 0.03$  m,  $L = W = 0.08$  m. The reason for such values is for the consideration of actual applications and the implementation of boundary conditions. In real situations, the interior tissue temperature usually tends to be constant within a short distance such as  $2 \sim 3$  cm ( $x$  direction) starting from the skin surface [3, 12, 17]. The computational domain size in the  $y$  and  $z$  directions are chosen to be fairly large so that the symmetric boundary condition, i.e., no heat flux goes in or out of the interested domain in the  $y$  and  $z$  directions, can be implemented. The material properties and parameters in Eq. (1) are  $\rho = \rho_b = 1000$  kg/m<sup>3</sup>,  $C = C_b = 4000$

J/(kg°C),  $T_a = T_c = 37$  °C,  $k = 0.5$  W/(m°C),  $w_b = 0.5$  kg/(m<sup>3</sup>s),  $Q_m = 33800$  W/m<sup>3</sup>. For simplicity, the surrounding fluid temperature is chosen as constant room temperature  $T_f = 25$  °C [12, 18]. The material properties related to Eq. (7) are  $G = 3.0 \times 10^6$  Pa,  $\nu = 0.25$ ,  $\nu_u = 0.31$ ,  $\alpha = 1.0 \times 10^{-4}$  °C.

#### 4.1 Case study: hyperthermia model

Hyperthermia is a heat treatment to biological body, a tool fairly often used in clinical applications such as tumor control by artificially elevating the tissue temperature to gain therapeutic benefits. The treatment of hyperthermia may be local, regional, or whole body, and the corresponding heating style varies, such as microwave heating, ultrasound heating, electrode heating, or thermal dose [19]. Even though hyperthermia is difficult to implement technically, its medical value has been shown in greatly improving the therapy performance by combining with radiation treatment [20]. A typical clinic application of hyperthermia is the treatment of cancer by selectively attacking deep-seated tumors with high temperature [21]. Due to the difference of heating sources, hyperthermia can be done either externally or internally. For example, the goal of standard hyperthermia treatments in internal heating is to raise the temperature in the target area to a higher degree, approximately 43 °C, than ordinary body temperature (37 °C) for up to one hour without excessively heating the adjacent tissues [22]. Patients usually do not feel comfortable with such a long time treatment. Another drawback of the standard procedure is the difficulty in accurately providing the desired thermal dose because of the possible changes of blood flow rates and thermal properties and hence the change of heat transfer mechanism between tissues and blood flow due to temperature variation. An alternative way is the short duration high temperature thermal treatments, known as high-temperature thermal therapy.

For simplicity, only point heating is considered to investigate the temperature response of tissue near tumor sites as did in some other research works [12, 18]. Practical examples of point heating can be found in clinical treatments where heat is deposited through inserting a conducting heating probe in the deep tumor site or delivering thermal dose to it. The point heating source to be studied is of the form [12]

$$Q_r(x, y, z, t) = P(t)\delta(x - x_0)\delta(y - y_0)\delta(z - z_0), \quad (12)$$

where  $P(t)$  is the strength of point heating source, which may vary with time,  $\delta$  the Dirac function, and  $(x_0, y_0, z_0)$  the location of point heating. In the present example, we investigate the tissue thermal response of three point heating, and the consequent effect of temperature change on the stress and displacement of the tissue concerned. The locations of the heating sources are all chosen in the same cross section at  $x = 0.009$ m, and the coordinates of the three points are (0.009, 0.032, 0.04)m, (0.009, 0.04, 0.028)m, and (0.009, 0.04, 0.028)m, the same as in the work demonstrated by Deng and Liu [18]. Among the three point heating sources, the heating strength is taken the same as  $P(t) = 1.0 \times 10^7$  W/m<sup>3</sup>. It is assumed that the tissue is cooled by convection at the skin surface. The convection coefficient is  $h_f = 100$  W/m<sup>2</sup> and the temperature of the cooling medium is  $T_f = 15$  °C.

The determination of heating style, heating location, and heat transfer parameters are solely for the purpose of convenience in presenting computational results and coherence in continuing research in this area, and they can be chosen as different values suitable for some applications consistent with the model.

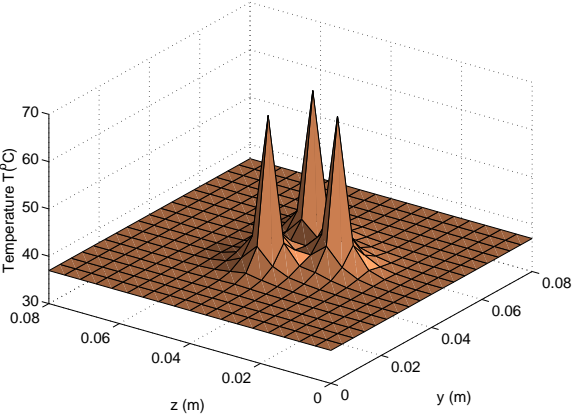


Figure 3: Temperature distribution at  $x = 0.09$  m and  $t = 200$  s (hyperthermia).

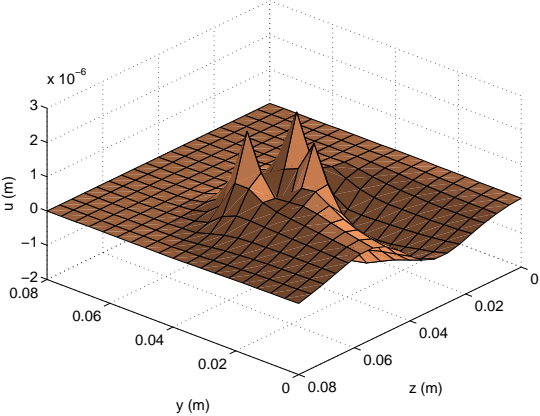


Figure 4:  $u$  displacement at  $x = 0.009$  m and  $t = 200$  s (hyperthermia).

In the quasi-steady state model, the time dependent thermomechanical responses can be achieved by solving the heat equation to get transient temperature distribution, and then solving the equilibrium equation to get displacement distribution based on the temperature at each time step. For brevity, only results in the  $(y - z)$  plane at  $x = 0.009$  m, where the three point heating sources locate, are displayed. Fig. 3 shows the temperature distribution at  $t = 200$  s, Figs. 4, 5, and 6 are the corresponding displacement distribution in the  $x$ ,  $y$ , and  $z$  space directions respectively.

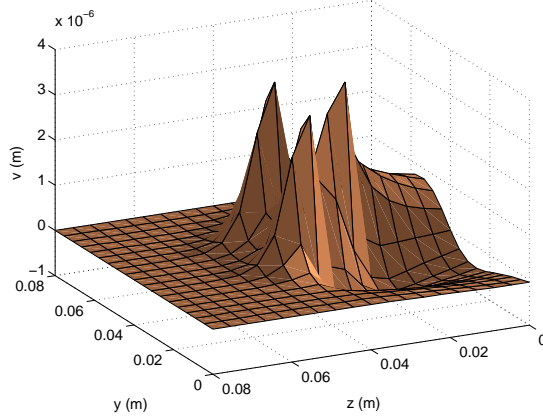


Figure 5:  $v$  displacement at  $x = 0.009$  m and  $t = 200$  s (hyperthermia).

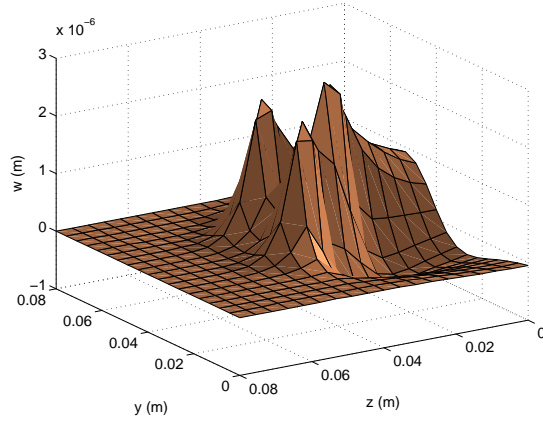


Figure 6:  $w$  displacement at  $x = 0.009$  m and  $t = 200$  s (hyperthermia).

The stress distribution is presented in Fig. 7 in the form of pressure  $\tilde{P}$  as

$$\tilde{P} = -\frac{\sigma_{xx} + \sigma_{yy} + \sigma_{zz}}{3}. \quad (13)$$

As shown in Fig. 3, the highest temperature is in the position where the heating source is placed, the same is true for the displacement (Figs. 4, 5, and 6) and stress (Fig. 7). It can be deduced without much difficulty that the tissue in the heated position is more likely to be damaged than that in locations which are not heated. This is what we expected in heat therapy by heating the target to a certain temperature to damage it and eventually kill it without major intervention to the neighboring healthy tissues.

The thermomechanical interaction has been presented at a fixed time  $t = 200$  s and different locations, as shown in Figs. 3 - 7. In the following space, we will show the thermal and mechanical properties at a fixed location but different time. For brevity, only the result at one of the three

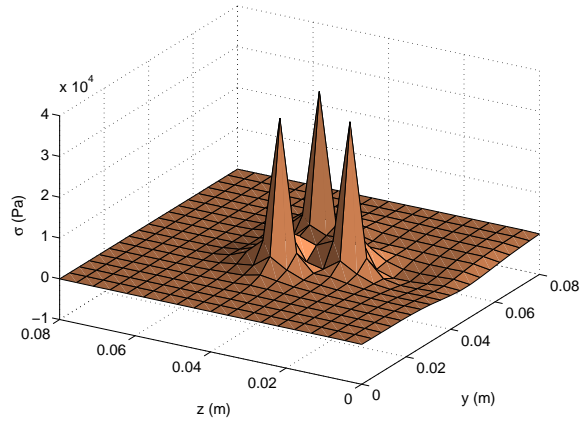


Figure 7: Average normal stress  $\tilde{P}$  at  $x = 0.009$  m and  $t = 200$  s (hyperthermia).

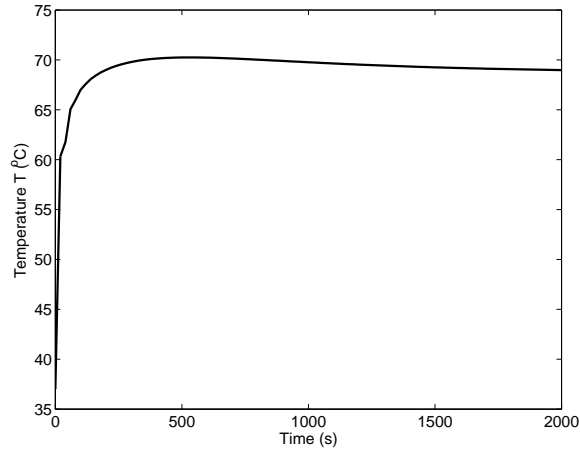


Figure 8: Transient temperature distribution at  $(0.009, 0.032, 0.04)$ m (hyperthermia).

positions where heating sources are located, i.e.,  $(x_0, y_0, z_0) = (0.009, 0.032, 0.04)$ m, is plotted, as displayed in Figs. 8 - 10. The variation of temperature with time is exhibited in Fig. 8, and that of stress is shown in Fig. 10. It can easily be seen that both temperature and stress have similar trend. That is probably because the thermal stress overwhelms mechanical stress in this particular case. The temperature increases rapidly in the early time of heating, reaches a peak value, then decreases gradually to become steady-state. That is because of the convection between the skin surface and the surrounding media with a lower temperature of  $T_f = 15$  °C. Fig. 9 is the change of displacement with time due to temperature difference. All three components of displacement increase with time first fast and then gradually.

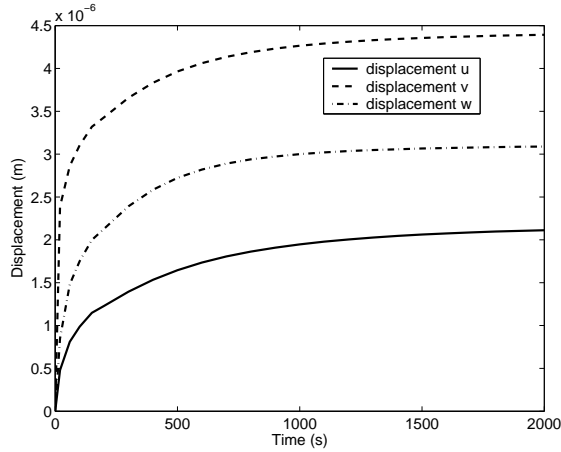


Figure 9: Transient displacement distribution at (0.009, 0.032, 0.04)m (hyperthermia).

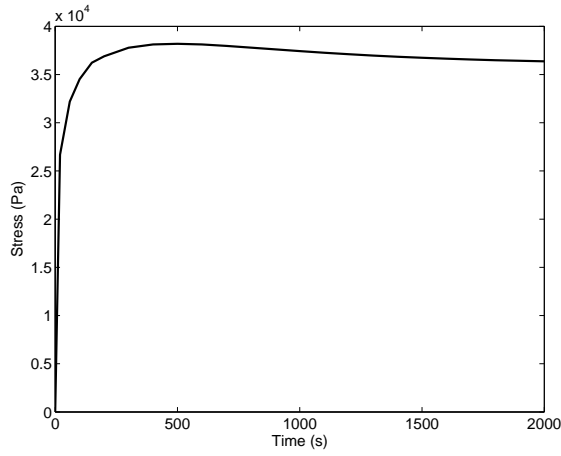


Figure 10: Transient average stress distribution  $\tilde{P}$  at (0.009, 0.032, 0.04)m (hyperthermia).

## 4.2 Case study: sinusoidal surface heating model

Oscillating heating is a quite common technique in thermal analysis, such as the application of modulated temperature programming to the investigation of thermomechanical interaction [24]. One example is the recent usage in thermogravimetry of modulated temperature programs to determine the degradation kinetics of materials. A sinusoidal temperature profile is the most common one among the various oscillating heating modulations. Sinusoidal surface heating can be generated by an instrument with repeated irradiation from regulated laser, and used to estimate the blood perfusion [25]. The sinusoidal heating is taken in the form of [18]

$$f(t) = q_0 + q_w \cos \omega t, \quad (14)$$

where,  $f(t)$  is heat flux ( $\text{W}/\text{m}^2$ ),  $q_0$  a constant,  $q_w$  the constant oscillation amplitude of sinusoidal heating,  $\omega$  the heating frequency. Eq. (14) is actually the flux on the skin surface provided by some

external devices. In computation, the sinusoidal heating is implemented by specifying a given heat flux boundary condition on the skin surface. The actual form of Eq. (14) is taken as

$$f(t) = 1000 + 500 \cos(0.02t). \quad (15)$$

The transient thermomechanical response in the case of surface heating are presented in Figs. 11 - 13. The temperature changes with time at the skin surface corresponding to Eq. (15) can be seen in Fig. 11. Because of continuous heating, the temperature on the skin surface increases gradually. It is clear, there are about six cycles in the history of temperature variation, which is due to the value of  $\omega$  in Eqs. (14) and (15). In the case of  $\omega = 0.02$ , the period of cosine function is  $100\pi$  seconds, and there are approximately six cycles in 2000 seconds. The thermal-induced displacement is shown in Fig. 12. Similar periodical changes can be observed. As expected, the magnitude of displacement variation is greatest for component  $u$ , since the temperature changes only in the  $x$  direction by the specified boundary conditions: symmetric in both the  $y$  and  $x$  directions. The thermal-induced stress also changes oscillatorily as displayed in Fig. 13.

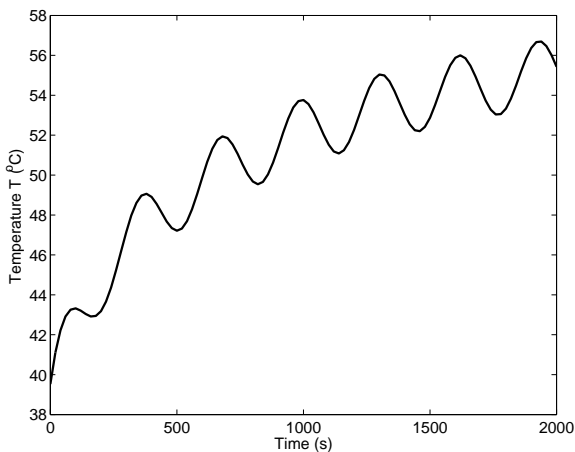


Figure 11: Transient temperature at skin surface (sinusoidal heating).

### 4.3 Computational Performance

Uniform grids were used in all the three space directions in numerical computation, also the same number of grid intervals are assigned in each of them. In the numerical examples done in both Sections 4.1 and 4.2, twenty equally spaced grid intervals are used, i.e.,  $19 \times 19 \times 19$  internal grid points. The consequent number of unknowns are  $57 \times 57 \times 57$ , as shown in Table 1. The information of the coefficient matrix  $A$  for the mesh size of  $39 \times 39 \times 39$  is included in Table 1 as well. The computation was done on a Sun-Blade-100 machine with a single 500 MHz SPARC processor and 2 GB memory.

Tables 2 and 3 present the computational performance with and without the ILUT preconditioner for two kinds of mesh sizes, i.e.,  $n = 6859$  and  $n = 59319$ , for the hyperthermia case study. In both cases, the parameters in the ILUT preconditioner are the same, i.e., drop tolerance

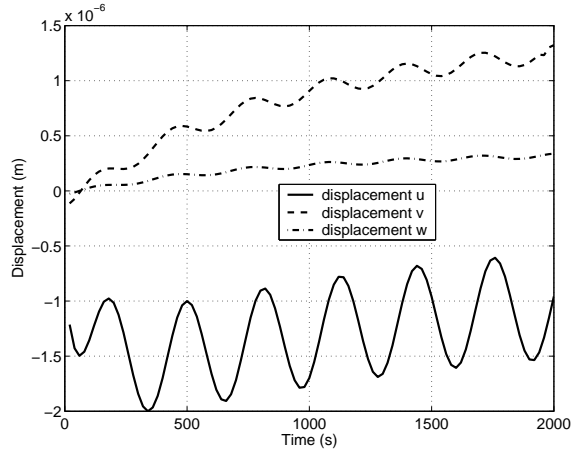


Figure 12: Transient displacement at skin surface (sinusoidal heating).

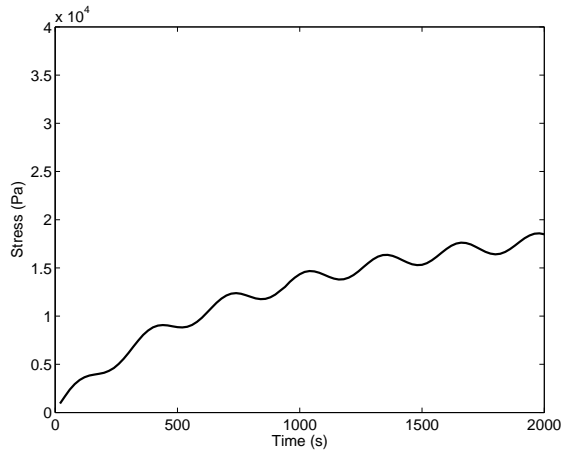


Figure 13: Transient average normal stress at skin surface (sinusoidal heating).

$\tau = 10^{-4}$ , level of fill-ins  $p = 40$ , and the size of the Krylov subspace is 50. It can be seen that the use of the ILUT preconditioners has greatly improved the computational performance. In the case of  $n = 6859$  (coarser grid), the number of iterations with the ILUT preconditioners is about eight times less than that without the preconditioner. In the case of  $n = 59319$  (finer grid), the number of iterations with the ILUT preconditioner is about fifty times less than that without the preconditioners. The total CPU time when using the ILUT preconditioner is less than a half of that without using the preconditioner in the coarser grid case, and about one fifth in the finer grid case. So the advantages of using the ILUT preconditioner are more remarkable when a finer grid discretization is used.

The influence of stop criterion on the computational cost is also studied in terms of number of iterations and CPU time. As shown in Tables 2 and 3, both the number of iterations and the total CPU time increase when the stop tolerance is changed from  $10^{-9}$  to  $10^{-12}$ .

Mesh size	No. of unknowns	No. of nonzeros
6859	20577	285285
59319	177957	2569905

Table 1: Information on matrix  $A$  for various mesh sizes (hyperthermia).

$n = 6859$	$\delta = 10^{-9}$		$\delta = 10^{-12}$	
	with ILUT	without ILUT	with ILUT	without ILUT
Computational cost	8	201	10	258
No. of iterations	7.85	-	7.71	-
Factorization time	9.48	20.59	9.73	27.20

Table 2: Computational performance with/without ILUT at  $n = 6859$  (hyperthermia).

## 5 Conclusion

Thermomechanical interactions were investigated in a three dimensional Cartesian coordinates. Pennes bioheat equation and the modified Duhamel-Neuman equations were proposed to model the thermal-induced mechanical behavior. We used the quasi-steady state thermoelasticity, where temperature and mechanical properties are not coupled and they are solved independently. The temperature is considered time-dependent, which is solved using a Crank-Nicolson numerical scheme. The mechanical properties themselves are not time-dependent, but they are related to temperature variations, so the transient mechanical properties such as displacement and stress can also be attained by solving them for various temperature distributions at each time step.

The heat equation was discretized using the standard 7 point central difference scheme, while the mechanical equilibrium equations were done by a 19 point finite difference scheme. Both of the schemes are second-order in accuracy. The resulting sparse linear systems from the discretization of both the heat transfer equation and the mechanical equilibrium equations are solved iteratively using GMRES solvers accompanied with the ILUT preconditioners. Both the number of iterations and the total CPU time are reduced in a great margin when the ILUT preconditioners are used.

Two numerical experiments were conducted, hyperthermia and sinusoidal heating, which represent typical heat transfer processes involved in soft tissues in biological bodies, such as heat therapy and skin burn. As expected, we obtained the time-dependent temperature distribution as well as the corresponding thermal-induced mechanical responses.

Based on the information presented in this paper, it is not difficult to draw a conclusion that the thermal-related mechanical properties can be modeled using the method suggested. The

$n = 59319$	$\delta = 10^{-9}$		$\delta = 10^{-12}$	
	with ILUT	without ILUT	with ILUT	without ILUT
Computational cost	9	452	11	542
No. of iterations	90.20	-	90.65	-
Factorization time	106.08	498.13	111.15	590.76

Table 3: Computational performance with/without ILUT at  $n = 59319$  (hyperthermia).

technique introduced here can be used to predict the outcome of a possible heat related medical therapy and estimate the damage to soft tissues due to the exposure to high temperature.

## References

- [1] Y. C. Fung, *Biomechanics Mechanical Properties of Living Tissues*, Springer-Verlag, New York, 1981.
- [2] H. H. Pennes, Analysis of tissue and arterial blood temperatures in resting human forearm, *J. Appl. Physiol.*, **1**, 93–122, 1948.
- [3] S. Weinbaum, L. M. Jiji, and D. E. Lemons, Theory and experiment for the effect of vascular microstructure on surface tissue heat transfer—part I: anatomical foundation and model conceptualization, *ASME J. Biomech. Eng.*, **106**, 321-330, 1984.
- [4] L. M. Jiji, S. Weinbaum, and D. E. Lemons, Theory and experiment for the effect of vascular microstructure on surface tissue heat transfer—part II: model formulation and solution, *ASME J. Biomech. Eng.*, **106**, 331-341, 1984.
- [5] M. M. Chen and K. R. Holmes, Microvascular contributions in tissue heat transfer, *Thermal Characteristics of Tumors: Applications in Detection and Treatment (Ann. New York Academy of Sciences, Vol. 335) (New York: Academy of Sciences)*, 137–150, 1980.
- [6] Y. C. Fung, *Foundations of Solid Mechanics*, Prentice-Hall, New Jersey, 1965.
- [7] J. W. Durkee Jr. and P. P. Antich, Exact solutions to the multi-region time-dependent bioheat equation with transient heat sources and boundary conditions, *Phys. Med. Biol.*, **36**, 345-368, 1991.
- [8] S. Tungjitkusolmun, S. T. Staelin, D. Haemmerich, J. Z. Tsai, H. Gao, J. G. Webster, F. T. Lee, Jr., D. M. Mahvi, and V. R. Vorperian, Three-dimensional finite-element analyses for radio-frequency hepatic tumor ablation, *IEEE Trans. Biomed. Eng.*, **49**, 3–9, 2002.
- [9] M. P. Cleary, Fundamental solutions for a fluid-saturated porous solid, *Int. J. Solids Structures*, **13**, 785–806, 1977.
- [10] A. N. Skempton, The pore pressure coefficients A and B, *Geotechnique*, **4**, 143–147, 1954.
- [11] J. Kubby, F. Yang, J. Ma et al., Bistable thermal actuators for switching applications, IP/A10795, Xerox Corp., June 2001.
- [12] S. Karaa, J. Zhang, and F. Yang, A numerical study of a 3D bioheat transfer problem with different spatial heating, Technical Report No. 372-03, Department of Computer Science, University of Kentucky, Lexington, KY, 2003.
- [13] Y. Saad and M. H. Schultz, GMRES: a generalized minimal residual algorithm for solving nonsymmetric linear systems, *SIAM J. Sci. Stat. Comput.*, **7**, 856–869, 1986.

- [14] Y. Saad, *Iterative Methods for Sparse Linear Systems*, PWS Pub., New York, 1996.
- [15] J. Lee, J. Zhang, and C. C. Lu, Incomplete LU preconditioning for large scale dense complex linear systems from electromagnetic wave scattering problems, *J. Comput. Phy.*, **185**, 158–175, 2003.
- [16] N. Kang, J. Zhang, and E. S. Carlson, Performance of ILU preconditioning techniques in simulating anisotropic diffusion in the human brain, *Future Generat. Comput. Sys.*, accepted.
- [17] J. Liu and L. X. Xu, Uncertainty analysis for temperature prediction of biological bodies subject to randomly spatial heating, *IEEE Trans. Biomed. Eng.*, **46**, 1037–1043, 2001.
- [18] Z. S. Deng and J. Liu, Analytical study on bioheat transfer problems with spatial or transient heating on skin surface or inside biological bodies, *ASME J. Biomech. Eng.*, **124**, 638–649, 2002.
- [19] H. S. Tharp and R. B. Roemer, Optimal power deposition with finite-sized, planar hyperthermia applicator arrays, *IEEE Trans. Biomed. Eng.*, **39**, 569–579, 1992.
- [20] R. B. Roemer, Engineering aspects of hyperthermia therapy, in *Annual Review of Biomedical Engineering*, M. L. Yarmush, K. R. Killer, and M. Toner, Eds., Palo Alto, CA, Annual Reviews, 347–376, 1999.
- [21] M. E. Kowalski, J. M. Jin, Model-order reduction of nonlinear models of electromagnetic phased-array hyperthermia, *IEEE Trans. Biomed. Eng.*, **50**, 1243–1254, 2003.
- [22] D. Arora, M Skliar, R. B. Roemer, Model-predictive control of hyperthermia treatments, *IEEE Trans. Biomed. Eng.*, **49**, 629–639, 2002.
- [23] J. W. Lee, K. S. Kim, S. M. Lee, S. J. Eom, and R. V. Troitsky, A novel design of thermal anomaly for mammary gland tumor phantom for microwave radiometer, *IEEE Trans. Biomed. Eng.*, **49**, 694–699, 2002.
- [24] D. M. Price, Modulated-temperature thermomechanical analysis, *J. Therm. Anal.*, **51**, 231–236, 1998.
- [25] A. T. Patera, B. B. Mikic, G. Eden, and H. F. Bowman, Prediction of tissue perfusion from measurement of the phase shift between heat flux and temperature, *Winter Annual Meeting of ASME, Advances in Bioengineering*, 187–191, 1979.
- [26] A. Ghassemi, A. Diek, and Helio dos Santos, Effects of ion diffusion and thermal osmosis on shale deterioration and borehole instability, AADE 2001 National Drilling Conference, Houston, Texas, 2001 (AADE01-NC-HO-40).